

# Quantitative Image Restoration

Irina Gladkova, Michael Grossberg, Fazlul Shahriar

## ABSTRACT

Even with the most extensive precautions and careful planning, space based imagers will inevitably experience problems resulting in partial data corruption and possible loss. Such a loss occurs, for example, when individual image detectors are damaged. For a scanning imager this results in missing lines in the image. Images with missing lines can wreak havoc since algorithms not typically designed to handle missing pixels. Currently the metadata stores the locations of missing data, and naive spatial interpolation is used to fill it in.

Naive interpolation methods can create image artifacts and even statistically or physically implausible image values. We present a general method, which uses non-linear statistical regression to estimate the values of the missing data in a principled manner. A statistically based estimate is desirable because it will preserve the statistical structure of the uncorrupted data and avoid the artifacts of naive interpolation. It also means that the restored images are suitable as input for higher-level statistical products.

Previous methods replaced the missing values with those of a single closely related band, by applying a function or lookup table. We propose to use the redundant information in multiple bands to restore the lost information. The estimator we present in this paper uses values in a neighborhood of the pixel to be estimated, and propose a value based on training data from the uncorrupted pixels. Since we use the spatial variations in other channels, we avoid the blurring inherent spatial interpolation, which have implicit smoothness priors.

## 1. INTRODUCTION

A common problem in satellite imagery is striping and scan line dropout. While transmission errors are sometimes the cause of this problem, a more frequent source is damage to individual detectors, or to the electronics that records the response of the detectors. Detectors are highly sensitive and precise elements, and despite extraordinary precautions and planning, damage is an unavoidable risk. Launch, deployment into the harsh environment of space, particle bombardment, radiation, and space dust can result in detector damage at any point of an imager's life cycle. When a damaged detector produces noisy or distorted data, this results in periodic stripes. The periodic nature comes from the fact that each detector is responsible for several scan lines within an image. When the data from the detector is absent or so corrupted as to be unusable, the result is periodic dropped lines.

There are many examples of imagers which suffer from periodic line drop. Classical examples include Landsat 4 and 5. More recent examples include the MODerate Resolution Imaging Spectrometer (MODIS) on Aqua. The 1.6 micron band (Channel 6) of the instrument has 15 broken or noisy detectors, out of 20. Figure 1 shows a portion of an Aqua image with the malfunctioning detectors shown as dark stripes. As can be seen, many of the malfunctioning detectors are adjacent so there are large spatial gaps in the data making spatial interpolation inappropriate. This limits its use in many potential applications such as cloud detection over bright surfaces such as snow and ice.

When faced with dropped scan lines, dummy values may be inserted to indicate lost data and the problem pixels are indicated in the metadata. While it is essential for end users to know which pixels represent reliable measurements, the presence of dummy values passes the burden of mitigating the data loss onto the end-user. Fundamental image processing operations such as 2D-convolution filters, or 2D Fourier transforms typically produce corrupt results if an image contains dummy values. To use standard image processing operations and off the shelf software, the missing data must be first estimated in some principled way. End users may have little or no knowledge of how to do that. It is important to note that many end users will often work with partial data, selected bands or regions of

interest. This both magnifies the impact of missing data and makes it harder to accurately compute a principled estimate.

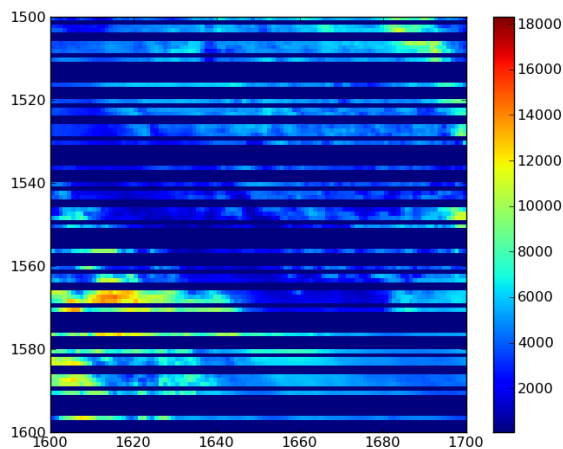


Figure 1. A portion of the MODIS/Aqua-Band 6 image showing striping due to broken detectors. Because many of the stripes are consecutive, naive interpolation is not appropriate for estimating the missing data.

## 2. RELATED WORK

There have been two previous approaches to propose to restore the damaged MODIS band 6 (1.6281.652 m) by Wang et. al in 2006, and Rakwatin et. al in 2009.<sup>1,2</sup> In Wang et. al, 2006,<sup>1</sup> the authors' motivation is to exploit the well known strong correlation bands 6 and bands 7. They show empirically that a polynomial regression can be used to determine a function from Terra band 7 radiances to Terra band 6 with relatively small mean squared error. By analyzing the coefficients of various regressions they reported good results for a cubic polynomial fit, while ruling out high order polynomials based on the extra coefficients showing little benefit. They then validated this relationship on the using the working sensors of Aqua band 6 to compare with simulated band 6 derived from the band 7 global cubic regression. A local cubic regression approach was proposed by Rakwatin et. al. in 2009.<sup>2</sup>

They use the working sensors of band 6, and the corresponding sensors of band 7, within a sliding window, to perform a locally varying cubic regression. This local regression is then applied to the band 7 data to restore the band 6 data at the damaged sensors. Note that although a window is used to find the coefficients of the polynomial regression, the input to the regression is just the band 7 value. In addition allowing the regression to vary across the image, they also applied histogram matching to the radiances to further improve the consistency of the regression and simultaneously reduce striping artifacts.

The fundamental problem with any approach that uses band 7 alone to determine band 6 is that depending on surface and cloud composition, these bands behave differently. While it may be true that on a generally uniform conditions the the assumption of a functional relationship may hold, these are also the situations where the restoration is least important. The sparse measurements provided by the working band 6 sensors alone may provide sufficient information on the interior of homogeneous regions. The mixed regions as well as boundaries between uniform regions such as snow lines or cloud edges are places where an accurate band 6 restoration can have the most impact. Also the input to the local regression is just the band 7 value at a point. If spatial variations in band 6 are not visible in band 7 at that point, they will not be reconstructed. While the pixel value at the corresponding point in band 7 alone cannot provide this information, we argue that with

multiple bands, and using local window as input (not just to train coefficients) can provide much more information to do the reconstruction.

We note that there are a number of methods to reconstruct missing information from an image. For example, *digital image inpainting* is often used to describe a kind of interpolation where the regions of missing data are so large that traditional interpolation fail. The variational and PDE based methods fill in missing data by finding the solution to a differential equation which is constrained by values surrounding the missing region. Examples of these methods can be found in the work of Ballester, Chan, and Bert.<sup>3-5</sup> These methods work well when the hole is relatively small and surrounded by large scale geometric structure. However, in the case where the surroundings of the hole consist of stochastic textures, such methods tend to produce blurred reconstructions and not to reproduce the texture. They also don't work well when the available undamaged data is sparse as it is in the case of band 6.

Another set of methods based on work in texture synthesis, generates plausible values within a missing region by randomly sampling from a probability distribution estimated from regions where the texture is assumed to be similar.<sup>6,7</sup> Such methods are inappropriate for the restoration of band 6 because we do not know, a priori, the class of texture that should be filled into band 6 where pixels are missing. In addition, the sparse values present in band 6, as well as the information in the other bands must condition the probabilistic sampling. These methods do not provide a means to do this. These methods also tend to fail on regions with large scale geometric structures like a coastline, or cloud edges. Exemplar based methods such as Criminis et al.<sup>8</sup> and Efros et al.<sup>9</sup> search for similar image patches, usually in the image surrounding the hole, and paste a filling of the hole using the found patches. Again the sparse data available from the working detectors of channel 6 makes this method inappropriate.

### 3. STATISTICAL ERROR MITIGATION ALGORITHM

In the case of MODIS/Aqua band 6, 15 out of 20 detectors are dead or unusable due to severe noise. The goal in the case of MODIS is to restore band 6 radiances using information from the sparse working detectors, and the radiances in related bands 3,4,5, and 7. The outline of the algorithm is presented in the diagram shown in Figure 2. The first step when working with the data is destriping the radiances. In theory the calibrated radiances should not have stripes. Nevertheless, some artifacts remain which can be removed using histogram specification.<sup>10</sup> As observed in Rakwatin et al.,<sup>2</sup> destriping can significantly improve regression.

After destriping, the image is then broken into disjoint non-overlapping large tiles consisting of  $I$  scanlines and  $J$  columns within a scanline, as shown in Figure 3. Reconstruction within each tile is accomplished with single multi-linear function which varies from tile to tile. It is also possible to use sliding overlapping tiles centered at the band 6 pixel to be restored, providing for a per-pixel varying reconstruction function. While a sliding window approach will potentially improve accuracy it does so at an enormous cost compared to non-overlapping tiles. Similarly, the choice of tile size is data-set dependent. Training data is used to find a balance between accuracy and speed, empirically, when setting the tile size.

Once the data is broken into fixed spatial tiles, sliding overlapping spatial windows of data within a tile are extracted as shown in Figure 3. The windows are of size  $m \times n$  pixels with  $m$  and  $n$  odd. In Figure 4 the pixels in stack of undamaged bands (Aqua 3,4,5,7) are considered independent (input) variables. The middle pixel the damaged band, Aqua band 6, is shown in Figure 3 as the dependent variable. For those spatial windows where the dependent variable corresponds to a pixel from a *working* band 6 detector, we have both independent variable values, and the dependent variable value. These pairs are fed into linear least squares regression as indicated in Figure 2. The result of the regression is a multi-linear map for each tile whose input is a stack of values in bands Aqua 3,4,5,7 within a window, and which computes a restored value at the center pixel in band 6. Again referring to Figure 2, the mapping for each tile is used to estimate the missing pixel value in Band 6, and with the pixel values from the working detectors in band 6, left intact.

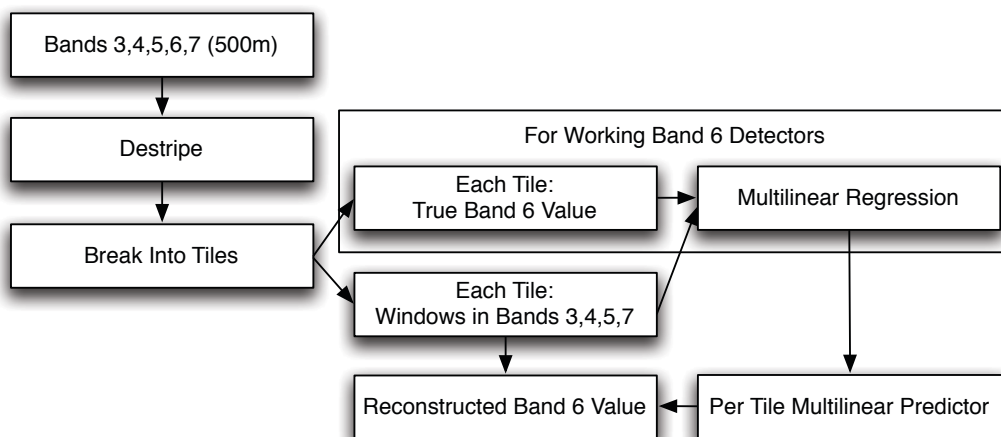


Figure 2. Block-diagram showing the steps of the reconstruction algorithm. Radiance values from working detectors in each band are destripped using histogram matching as a pre-processing step. The entire image is broken into non-overlapping tiles with the tile size chosen empirically. Within each tile, for each pixel value corresponding to a working band 6 detector, a surrounding geometric window of surrounding is defined. Values from pixels within geometric window measured in bands 3,4,5 and 7 are treated as independent variables, with the single band 6 value as a dependent variable to set up a multi-linear regression. The coefficients determined by the regression are then applied to the window of values measured in bands 3,4,5 and 7 to estimate the missing values in band 6.

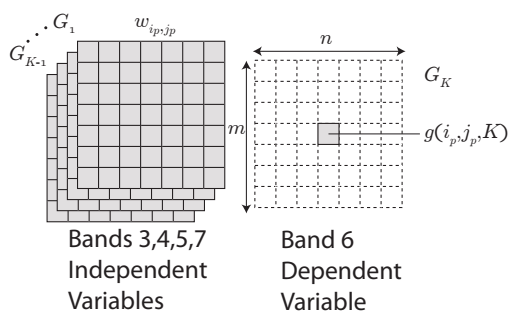


Figure 3. Diagram of the spatial arrangement of pixels used for prediction

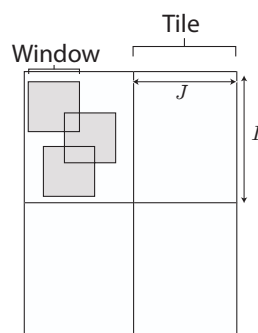


Figure 4. View multi-spectral/spatial neighborhoods considered for prediction

More formally, we can generalize the algorithm to take  $K$  bands, where, by renumbering we can assume 1 through  $K - 1$  are working bands and band  $K$  is the band to be restored. Since each  $I$  by  $J$  tile is treated independently, we fix one such tile. Within that tile we represent a discrete image as an integer-valued function  $g(i, j, k)$ , with values in the range is  $[0, 2^b - 1]$ , with  $b$  the bit-depth of the instruments, and  $1 \leq i \leq I$ ,  $1 \leq j \leq J$ , and  $1 \leq k \leq K$ . With this representation, an image from the  $k$ th band is the restricted function  $G_k(i, j) = g(i, j, k)$ . From this point of view,  $G = \{G_k\}_{k=1}^K$  can be considered as a stack of 2D images, one for each band  $k$ .

The correlations in nearby the spectral and spatial values the window centered at the location  $(i_p, j_p)$  provide correlations which can be used to estimate the center pixel. We represent the local input context as a window  $w_{i_p, j_p}$  defined by

$$\mathbf{w}_{i_p, j_p} = \{g_{i,j,k} | i_p - m/2 < i < i_p + m/2, j_p - n/2 < j < i_p + n/2, \text{ and } 1 \leq k \leq K - 1\}, \quad (1)$$

where  $(i_p, j_p)$  represents the middle pixel, see Figure 4. Also shown in Figure 4, is the dependent value  $g(i_p, j_p, K)$ , which either comes from (in training data) the working detectors, or  $(g(i_p, j_p, K))$  must be determined.

The reconstruction itself is a function  $F(\mathbf{w}_{i_p, j_p})$  so that  $F$  minimizes  $|F(\mathbf{w}_{i_p, j_p}) - g(i_p, j_p, K)|^2$  in the least squares sense. For a sensible reconstruction of this form to even be possible, the points  $(w_{i_p, j_p}, g(i_p, j_p, K))$  in  $K$  dimensions should lie close to some surface which is singled valued in the first  $K - 1$  dimensions. We approximate this surface with a plane which for each tile.

By a plane, we mean that we consider a parameterized family of reconstruction multi-linear functions  $F_\alpha$  with

$$F_\alpha(\mathbf{w}_{i_p, j_p}) = \mathbf{w}_{i_p, j_p} \cdot \alpha \quad (2)$$

where the values of  $\mathbf{w}_{i_p, j_p}$  are treated as a  $nm(K-1)$  vector,  $\alpha$  is a vector of  $nm(K-1)$  coefficients, and  $F_\alpha(\mathbf{w}_{i_p, j_p})$  is the scalar dot product. The parameters  $\alpha$  are determined independently on each tile to minimize the sum of square differences (SSD)

$$SSD(\alpha) = \sum_{p \in W} |F_\alpha(\mathbf{w}_{i_p, j_p}) - g(i_p, j_p, K)|^2. \quad (3)$$

where  $W$  is the set of pixels where the detectors in the  $K$ th band are functioning normally and so  $g(i_p, j_p, k)$  is known. The solution to this minimization, least-squares, is exact and is easily determined.<sup>11</sup> Once the parameters  $\alpha$  are determined for a tile, all the missing values in band  $K$  are replaced using  $F_\alpha(\mathbf{w}_{i_p, j_p})$ .

Note that in the algorithm just described we do not explicitly utilize the values coming from functioning band 6 pixels after the parameters are determined for a tile, all the missing values in band  $K$  after the parameters  $\alpha$  have been determined. In special cases we can extend the previous algorithm by appending the values from the working detectors in band  $K$  within the  $m \times n$  window to the vector  $\mathbf{w}_{i_p, j_p}$ . For instance, if the detector loss is given by alternating lines then there are two classes of band  $K$  sliding windows within a tile: those whose top line consists of working detectors and those whose top line does not. In this case we can minimize Eq. 3 separately for each case yielding two regression functions for each tile. In greater generality, the same technique can, in theory be applied. Unfortunately in practice, when the detectors damaged has a more complex periodic pattern such as in the case of MODIS/Aqua, the number of separate minimizations grows per tile. As a result there are less windows per tile per minimization to use in training degrading performance. Thus we only present here the case where  $\mathbf{w}_{i_p, j_p}$  values come from the first  $K - 1$  bands. In future work we plan to test the extended algorithm for a data set where it can be applied.

### 3.1 Implementation

The algorithm was implemented using the Python programming language, and it's Numpy/Scipy linear algebra package. The MODIS data in HDF4 format are read in using the PyHDF library, which is a wrapper around the C HDF library from HDF Group. The library was fast enough that it allowed direct use of the raw data from disk, even when the data units were being converted to radiances. All the graphics were created with Python's Matplotlib package.

#### 4. RESULTS

While we have already described the extensive damage to band 6 detectors of MODIS/Aqua, the corresponding band 6 of the MODIS/Terra has no such problem. This makes it possible to use the evaluate the algorithm by simulating the band 6 MODIS/Aqua damage on MODIS/Terra. This allows us to then compare the restored values with ground truth. The following table 5 shows a selection of 14 randomly chosen granules with the root mean square error for the restoration:

| Granule name (MOD02HKM.)        | RMSE  |
|---------------------------------|-------|
| A2003256.0400.005.2009234182813 | 0.367 |
| A2004360.1735.005.2008257130038 | 0.338 |
| A2005005.1225.005.2009313213947 | 0.319 |
| A2005327.0230.005.2009313214459 | 0.481 |
| A2006033.1030.005.2008274152905 | 0.269 |
| A2007002.2245.005.2009313214438 | 0.372 |
| A2007354.1045.005.2007354223142 | 0.301 |
| A2008290.0720.005.2009313214219 | 0.446 |
| A2008361.1020.005.2008361201900 | 0.543 |
| A2009062.1550.005.2009063012701 | 0.508 |
| A2009077.1505.005.2009078022408 | 0.620 |
| A2009119.0935.005.2009313213631 | 0.150 |
| A2009152.0640.005.2009152134621 | 0.275 |
| A2009162.1700.005.2009163141647 | 0.752 |

Figure 5. Root Mean Square Error for the restoration.

Given the large number of detectors lost these RMSE are quite low across granules. Even within a granule the spread of errors is quite narrow. Figure 6 shows the histogram of errors using 5x5 windows within the tiles. Most of the errors are tightly concentrated around zero. We found that indeed breaking the data into tiles and determining the linear regression on these tiles did improve the the error. For instance on the granule MOD02HKM.A2009055.1720.005 if we a apply the per-tile regression with 3x3 windows we obtain an RMSE of 0.235. If we instead try to build a single linear regression for the whole granule with 3x3 patches, the RMSE drops to 0.502.

The performance of the algorithm with increasing window size improves slightly from 3x3 to 5x5 windows, but after that either shows no improvement or actually degrades with increasing window size as shown by the solid average curve in Figure 7. The figure also shows that when examining different portions of a granule, there can be a wide variation in performance depending on scene structure.

Figure 8 shows two curves obtained by averaging the restoration results when the data is first destriped, and when it is used without destriping. There is a clear advantage to using destriping. In the curve of errors without destriping we see that the error using larger and larger windows increases much more rapidly then when the image is destriped. This is because as the windows become large the different possible relative locations of the stripes within the windows effectively add noise to the input space degrading the performance of the restoration. Another factor that contributes to the effectiveness of the restoration is the number of working sensors. The algorithm clearly degrades as the number of working sensors decreases as shown in Figure 9. Note that when there are no working detectors the algorithm still is able to estimate the missing band from the other detectors, admittedly, with a much larger error.

We can compare our restoration to the restoration currently used by NASA which is a column-wise interpolation. Figure 10(a) shows a band 6 MODIS/Terra image with simulated band 6 aqua

damage and column-wise interpolation identical to that used by NASA on MODIS/Aqua band 6, with a detail in the lower right. Strong artifacts of interpolation are clearly visible. Figure 10(b) shows the same portion of the band 6 granule normally, as obtained from band 6 MODIS/Terra with corresponding detail. Figure 10(c) shows our restoration of Aqua band 6. Note, the complete lack of obvious artifacts.

The artifacts of column-wise interpolation are particularly striking when considering the the gradient of the images. Gradients are critical at detecting boundaries of change and reveal a great deal of image structure. Figure 11(a)-(c) shows the magnitude of the gradients corresponding to the same images in Figure 10(a)-(c). Clearly the artifacts of column-wise interpolation are magnified. Even though the gradient will magnify noise and artifacts, our restoration still shows little or no artifacts in the gradient images, and compares well with ground truth.

As further qualitative evaluation, the original Terra data shown in Figure 13 appears nearly identical to that of our restoration Figure 14, where the scene contains heavy clouds as well as linear cloud structures. Similarly the original image shown in Figure 15 and the restored image in Figure 16 look nearly identical but here we see light cloud and sharp ground based structures such as rivers.

In the case of MODIS/Aqua data we do not have ground truth available. Still we can compare the results that are currently produced with interpolation in Figure 17, with our reconstruction as can be seen and the reconstruction we produce in Figure 18. Note that fine structure are visible and thought we do not know the true scene appearance, the reconstructed data lacks the strong artifacts of the interpolated results. Similar to the prior terra example with linear cloud structures, those structures are distorted in Figure 19 while well reconstructed in Figure 20.

## 5. CONCLUSIONS

We have shown that using all the neighboring channels we are able to quantitatively estimate the value at dead or noisy detectors. This work can provide a valuable risk mitigation tool for damage and failure of remote sensors. Future work will apply these ideas to other sensors with damaged detectors. We plan to evaluate the benefits on higher order products that use MODIS band 6 such as snow and cloud masks.

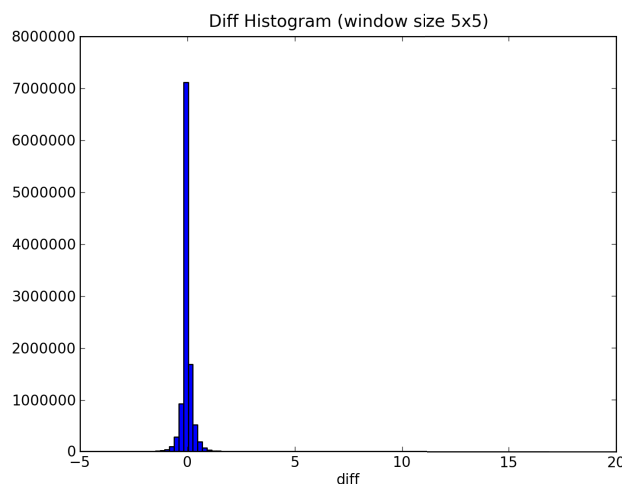


Figure 6. This shows the distribution of errors for a restoration of a band 6 from Terra with simulated damage using 5x5 windows. Note that the errors are well concentrated about 0.

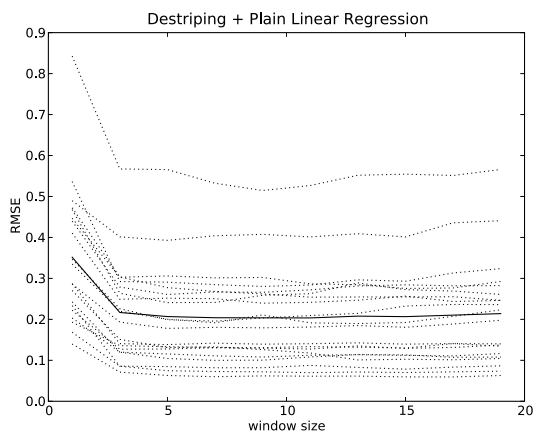


Figure 7. Graph showing RMSE for the algorithms with different window sizes. This shows the wide variance performance when the algorithm is restricted to different regions within a granule as represented by the dotted line. The average is represented by the solid line and shows that after a window size of 5x5 there is little improvement

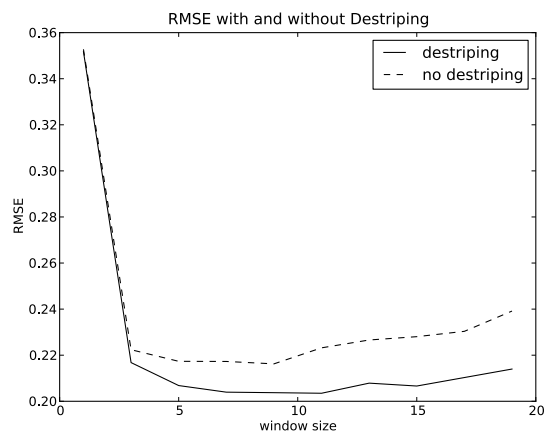


Figure 8. Graph demonstrating the impact of destriping on restoration. Without destriping not only does the error increase, but larger windows become increasingly problematic. The strip pattern on larger windows will be more complex and thus create degrading results during regression.

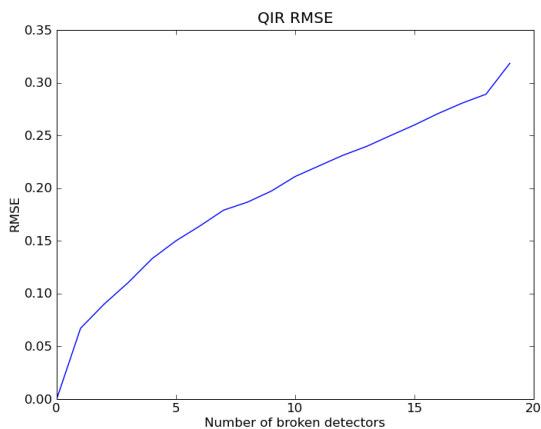


Figure 9. Diagram showing how error increases with fewer and fewer working detectors. Even with no working detectors, some estimate of the band although the training data in this case

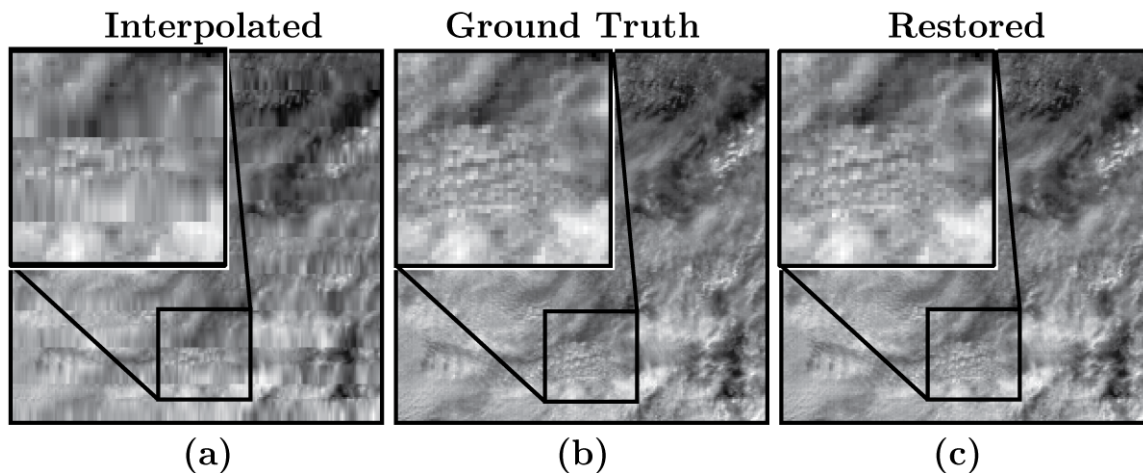


Figure 10. Comparison of the restoration when compared to column wise interpolation. In (a) Terra MODIS band 6 has been damaged to match the damage in Aqua MODIS band 6 and then interpolated. The artifacts of the interpolation are clear in both the image and the magnified inset. In (b) the image is the original Terra image as ground truth. (c) The restored image has none of the artifacts and looks nearly identical to the ground truth particularly when comparing the magnified insets.

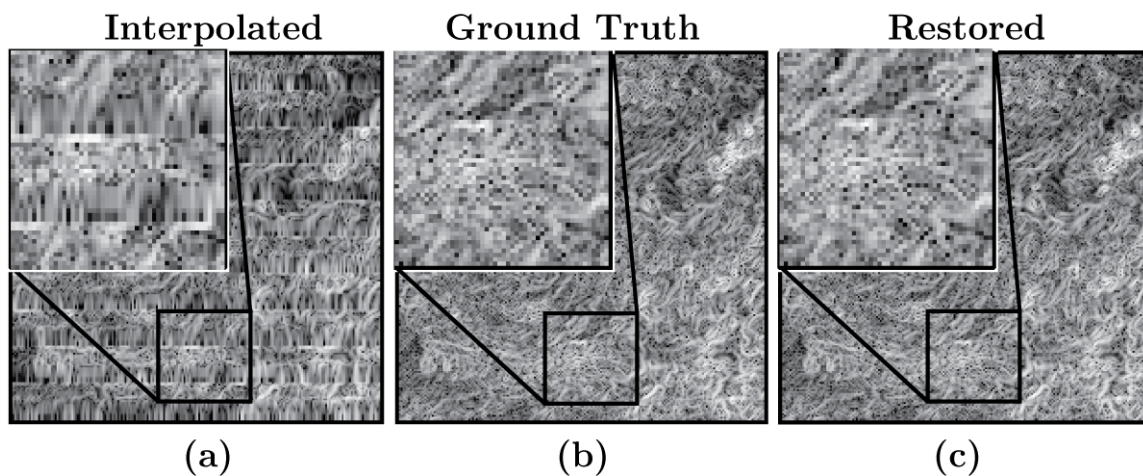


Figure 11. Same diagram as above where the magnitudes of the gradients are compared. The differences between the magnitude of the gradient image coming from column-wise interpolation is radically different from the magnitude gradient of the original image. In contrast the magnitude gradients of the restored image is nearly identical to that of the original image.

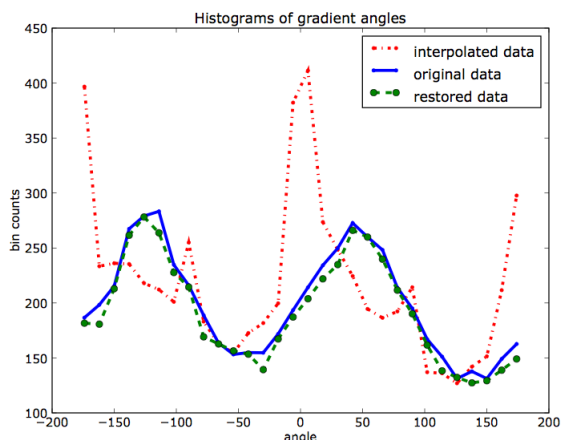


Figure 12. Histograms of image gradient angles from MODIS/Terra band 6. MODIS/Terra band 6 functions normally and can thus be used to evaluate the restoration algorithm. The dotted line shows the distribution of image gradient angles when the NASA column-wise linear interpolation used to fill in Aqua band 6 is applied to Terra with simulated Aqua damage. As can be seen this creates strong artifacts periodic artifacts not present in the original data when compared with the solid line representing Terra ground truth. The dashed plot with round markers shows the distributions that result when our restoration is used. Note the close agreement ground truth.

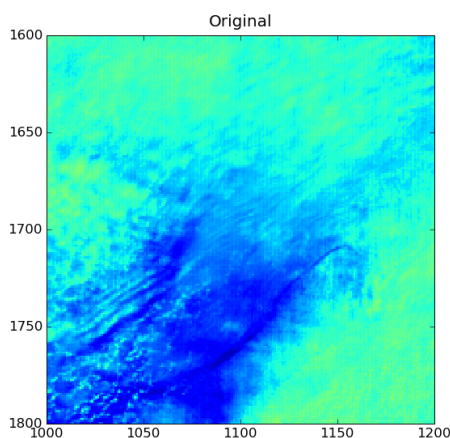


Figure 13. Original MODIS Band6 Terra Image with Cloud Structure. Note the linear structures in the clouds that should be reproduced in the restoration.

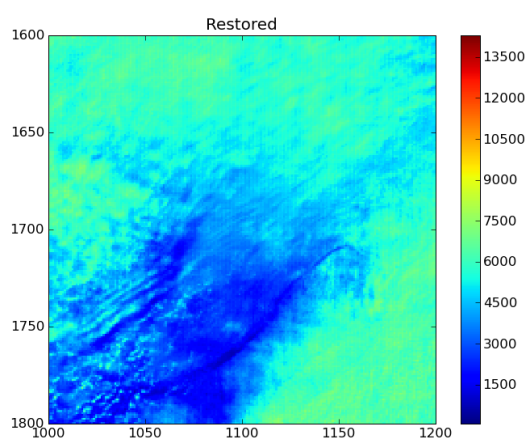


Figure 14. MODIS Band 6 Terra Restored Cloud image. After simulated damage the restoration algorithm we have presented is applied. Note how faithfully it captures the edge structure in the clouds.

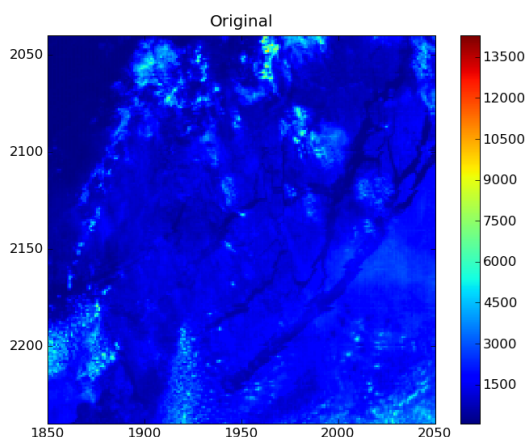


Figure 15. Original MODIS Band6 Terra Image with Surface Structure. Within the image small several rivers and tributaries are visible.

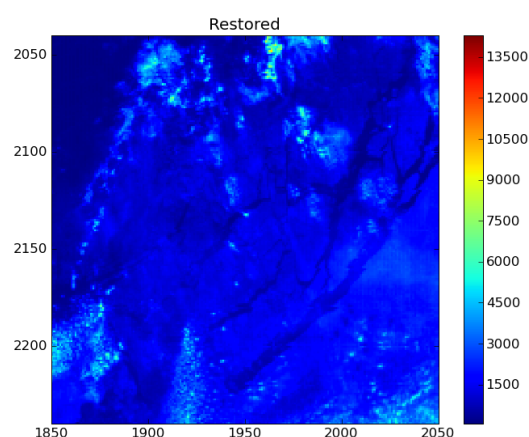


Figure 16. MODIS Band 6 Terra Restored Surface image. The restored image recovers the river and surface edge features without distortion.

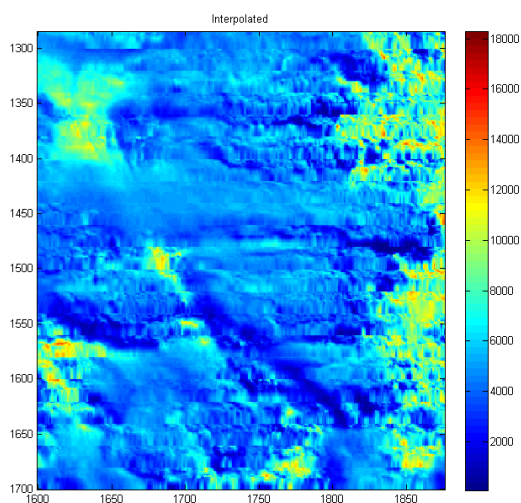


Figure 17. Band 6 MODIS/Aqua image with missing data column-wise interpolated. Even though ground truth is not available for Aqua images, the cloud detail in the upper right obvious artifacts the interpolation.

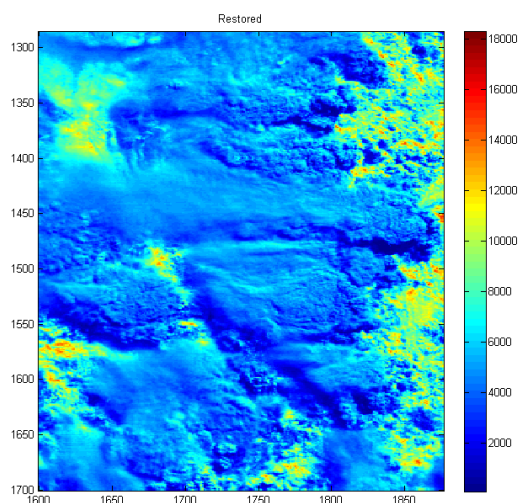


Figure 18. Restored Band 6 image shown. The upper right corner does not have the artifacts of the previous image. In the restored images there are no signs of obvious artifacts and the details are consistent with that of comparable images from Terra.

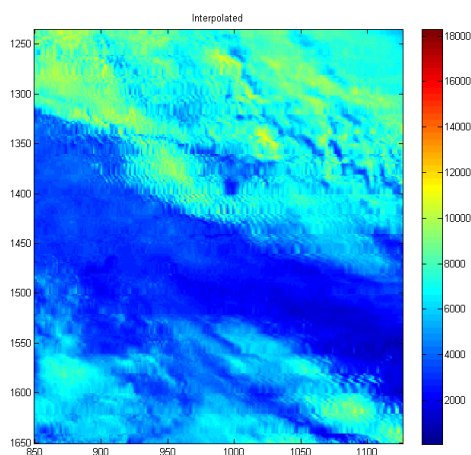


Figure 19. Band 6 MODIS/Aqua image with missing data column-wise interpolated. The image shows a 400 pixel x 200 pixel patch. Linear structures such as the clouds in the upper left are severely distorted by the interpolation. Diagonal edges appear as staircase like structures.

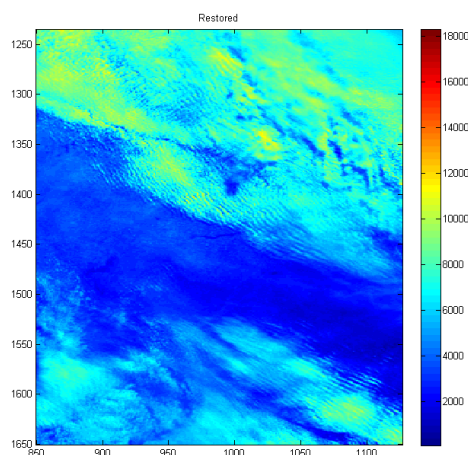


Figure 20. Restored Band 6 image shown. The staircase edges of the previous image are gone. Edges of clouds in any orientation appear sharp. The image can now be processed with off the shell image processing tools without worrying about lost data, or the impact of strong artifacts corrupting the image analysis.

## REFERENCES

1. L. Wang, J. Qu, X. Xiong, X. Hao, Y. Xie, and N. Che, "A new method for retrieving band 6 of Aqua MODIS," *IEEE Geoscience and Remote Sensing Letters* **3**(2), pp. 267 – 270, 2006.
2. P. Rakwatin, W. Takeuchi, and Y. Yasuoka, "Restoration of Aqua MODIS band 6 using histogram matching and local least squares fitting," *IEEE Transactions on Geoscience and Remote Sensing* **47**(2), pp. 613 – 627, 2009.
3. C. Ballester, M. Bertalmio, V. Caselles, G. Sapiro, and J. Verdera, "Filling-in by joint interpolation of vector fields and gray levels," *IEEE Trans. Image Proc.* **10**(8), pp. 1200–1211, 2001.
4. M. Bertalmio, A. Bertozzi, and G. Sapiro, "Navier-stokes, fluid dynamics, and image and video inpainting," in *Conference on Computer Vision and Pattern Recognition, ACM* **1**, pp. 355–362, 2001.
5. T. Chan, S. Kang, and J. Shen, "Euler's elastica and curvature-based inpainting," *SIAM J. Appl. Math* **63**(2), pp. 564–592, 2002.
6. S. Zhu, Y. Wu, and D. Mumford, "Filters, random fields, and maximum entropy (frame): Towards a unified theory for texture modeling," *Int. J. Comput. Vis.* **27**(2), pp. 107–126, 1998.
7. D. Gustavsson, K. Pedersen, and M. Nielsen, "Image inpainting by cooling and heating," in *Scandinavian Conference on Image Analysis*, B. Ersboll and K. Pedersen, eds., *Lecture Notes in Computer Science* **4522**, pp. 591–600, Springer, Berlin, 2007.
8. A. Criminisi, P. Perez, and K. Toyama, "Region filling and object removal by exemplar-based image inpainting," *IEEE Trans. Image Proc.* **13**(9), pp. 1200–1212, 2004.
9. A. Efros and W. Freeman, "Image quilting for texture synthesis and transfer," in *Proceedings of SIGGRAPH*, (Los Angeles, California, USA), August 2001.
10. J. S. Cheng, Y. Shao, H. D. Guo, W. Wang, and B. Zhu, "Destriping CMODIS data by power filtering," *IEEE Trans. on Geoscience and Remote Sensing* **49**, pp. 2119 – 2124, 2003.
11. W. Press, B. Flannery, A. Teukolsky, and W. Vetterling, *Numerical Recipes in C: The Art of Scientific Computing*, Cambridge University Press, 1992.